ACS APPLIED MATERIALS & INTERFACES
Research Article
www.acsami.org

$BaTiO_3$ Integration with Nanostructured Epitaxial (100), (110), and (111) Germanium for Multifunctional Devices

Mantu K. Hudait,*,† Yan Zhu,† Nikhil Jain,† Deepam Maurya,‡ Yuan Zhou,‡ Ron Varghese,‡ and Shashank Priya‡

†Advanced Devices & Sustainable Energy Laboratory (ADSEL), Bradley Department of Electrical and Computer Engineering, ‡Center for Energy Harvesting Materials and Systems (CEHMS), Virginia Tech, Blacksburg, Virginia 24061, United States

ABSTRACT: Ferroelectric−germanium heterostructures have a strong potential for multifunctional devices. Germanium (Ge) is attractive due to its higher electron and hole mobilities while ferroelectric $BaTiO_3$ is promising due to its high relative permittivity, which can make next-generation low-voltage and low-leakage metal-oxide semiconductor field-effect transistors. Here, we investigate the growth, structural, chemical, and band alignment properties of pulsed laser deposited $BaTiO_3$ on epitaxial (100)Ge, (110)Ge, and (111) Ge layers. Cross-sectional transmission electron microscopy micrographs show the amorphous nature of the $BaTiO_3$ layer and also show a sharp heterointerface between $BaTiO_3$ and Ge. The appearance of strong Pendellösung oscillation fringes from high-resolution X-ray diffraction implies the presence of parallel and sharp heterointerfaces. The valence band offset relation of $\Delta E_V(100) \geq \Delta E_V(111) > \Delta E_V(110)$ and the conduction band offset relation of $\Delta E_C(110) > \Delta E_C(111) \geq \Delta E_C(100)$ on crystallographically oriented Ge offer significant advancement for designing new-generation ferroelectric−germanium-based multifunctional devices.

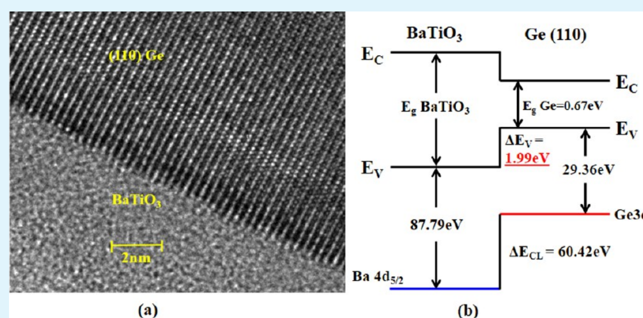

KEYWORDS: *germanium, barium titanate, X-ray photoelectron spectroscopy, band offsets, molecular beam epitaxy*

■ INTRODUCTION

Perovskite−semiconductor heterostructures have been attractive due to the potential for optoelectronic, electronic, and memory devices.[1−11] Among all perovskite materials, $BaTiO_3$ (BTO) has been widely studied for integration with semiconductors, and also, it has a high relative permittivity that can be used as the gate dielectric in a next-generation metal-oxide semiconductor field-effect transistor (MOSFET) to reduce the operating voltage and minimize the gate leakage. In fact, BTO has been used as a part of the gate dielectric in Si MOSFET to reduce the subthreshold swing and increase the ON current with the drawback of hysteresis in the output characteristics of a transistor,[12,13] to control the free carrier concentration in the ZnO channel,[3,6] as a BTO/InN heterojunction for optical and electrical devices,[1] and for 6× reduction of gate leakage current in BTO/Ge MOS capacitor.[10] To use BTO as a gate dielectric to continue transistor miniaturization in the channel length down to a 5 nm gate length according to the International Technology Roadmap for Semiconductors,[14] low band gap channel materials with superior transport properties are required to achieve a further increase in transistor drive current in a nanoscale transistor. Furthermore, large offsets between the BTO and the channel materials are mandatory to minimize the gate leakage in a nanoscale MOSFET.

Germanium (Ge) has a great potential due to its higher electron and hole mobilities in conjunction with the BTO gate dielectric, which will enhance the carrier transport properties in a nanoscale transistor. It has low field bulk mobility gains up to 2× for electrons and 4× for holes compared with Si. The transistors fabricated on (110)Ge exhibited a hole mobility of 650 $cm^2/(V\ s)$[15] and higher electron mobility in the (111)Ge orientation than (100)Ge.[16] Moreover, the hole mobility in the (110)Ge channel orientated along the ⟨110⟩ direction exhibited 2.3× higher compared with (100)Ge,[17] and the electron mobility in the (111)Ge orientation is 1.8× higher than the electron mobility in both (100)Ge and (110)Ge orientations.[18,19] Furthermore, Ge can be used as a template on Si for III−V heteroepitaxy, and recent successful integration of high-κ gate dielectric on Ge,[20,21] which eliminates the unwanted low-κ interfacial dielectric layer than on Si, warrants the favorable choice for next-generation low-power transistors to continue Moore's law.

Significant research has been conducted on the integration of high-κ gate dielectrics such as HfO_2, ZrO_2, Al_2O_3, BTO and their band alignment with respect to (100)Ge,[21−27] (110)-Ge,[20,21,27,28] and (111)Ge[21,27] by several groups and including our own work. These band offset parameters are most important in oxide/semiconductor heterostructure devices to minimize the gate leakage currents. Among these new high-κ dielectric materials, higher-κ dielectric BTO material directly

Received: August 30, 2013
Accepted: October 17, 2013
Published: October 17, 2013

 © 2013 American Chemical Society

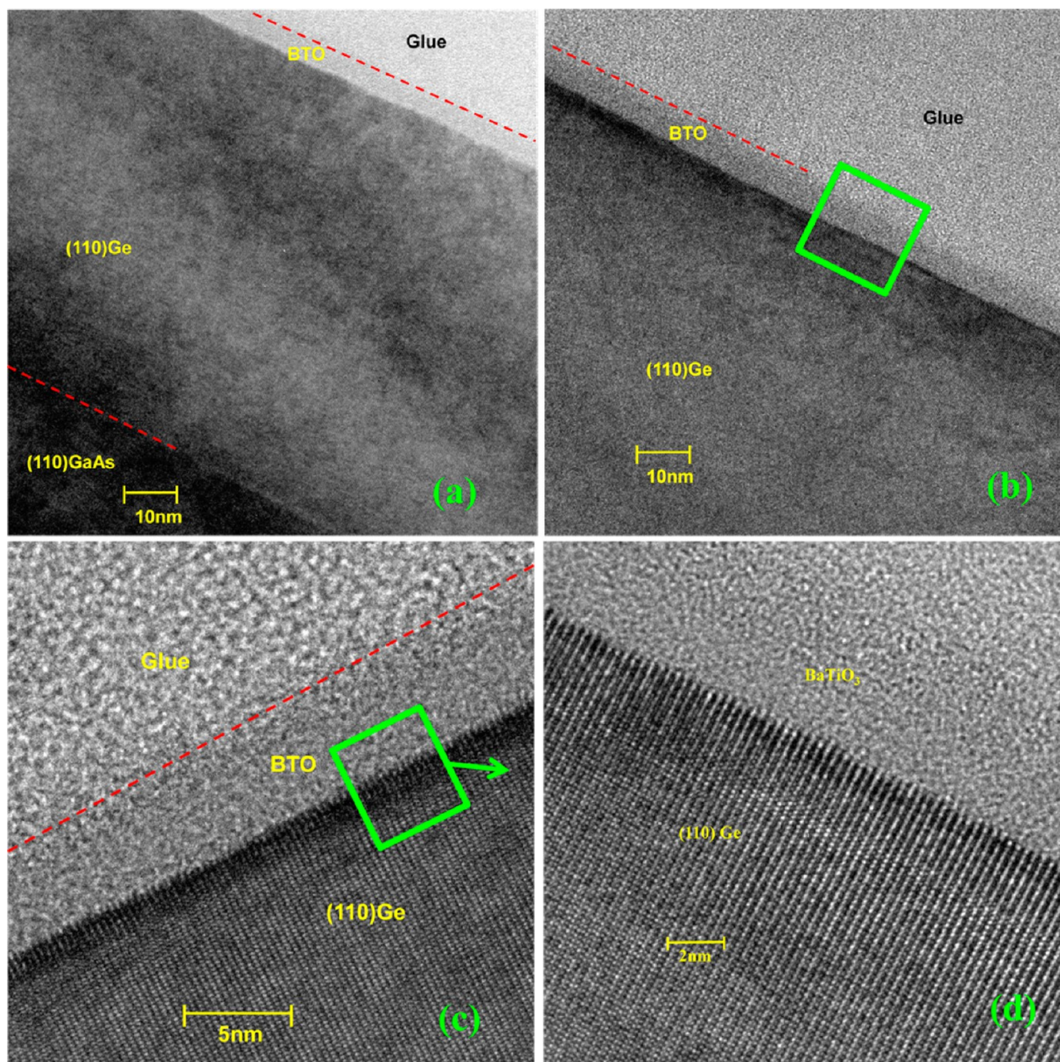

Figure 1. (a) Cross-sectional TEM micrograph of $BaTiO_3$ layer deposited on epitaxial (110)Ge grown on (110)GaAs substrate. (b) Uniform thickness of BTO in a relative long range. (c) BTO/(110)Ge interface. (d) High-resolution TEM micrograph at the $BaTiO_3$/(110)Ge interface. Sharp heterointerfaces between $BaTiO_3$/(110)Ge and Ge/(110)GaAs were demonstrated.

grown on (100)Si or (100)Ge showed negligible conduction band offset[10,25,26,29] and thus ruled out the possibility of a common gate dielectric solution for both p-channel and n-channel MOSFETs. However, up-to-date, there is a lack of experimental band offset data available at the BTO and different crystallographically oriented epitaxial Ge layers. It is important to know the band offset values that could select a common gate dielectric for n- and p-channel Ge MOS transistors. Furthermore, integration of BTO on crystallographically oriented Ge layers continues to be of interest for added functionalities on Ge for low-power CMOS logic applications. *In this paper,* we demonstrate the growth and band alignment properties of pulsed laser deposited (PLD) BTO on epitaxial (100)Ge, (110)Ge, and (111)Ge layers using molecular beam epitaxy (MBE) and X-ray photoelectron spectroscopy (XPS). The valence and conduction band discontinuities, ΔE_V and ΔE_C, larger than 1 eV[25] for BTO/Ge heterojunction are imperative to act as a blocking barrier for both holes and electrons.

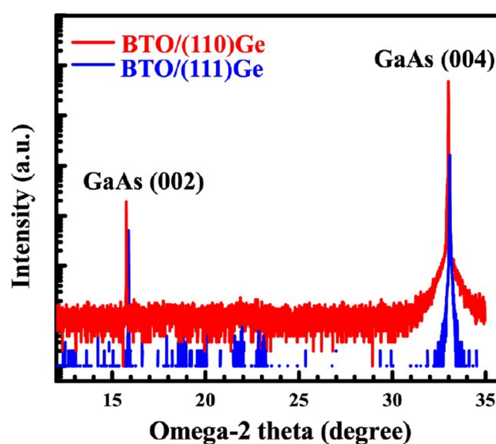

Figure 2. X-ray rocking curves from 5 nm $BaTiO_3$/80 nm (110)Ge and 5 nm $BaTiO_3$/80 nm (111)Ge structures on (110)GaAs and (111)A GaAs substrates, respectively. X-ray rocking curve does not exhibit a BTO peak, which suggests the amorphous nature of the BTO layer.

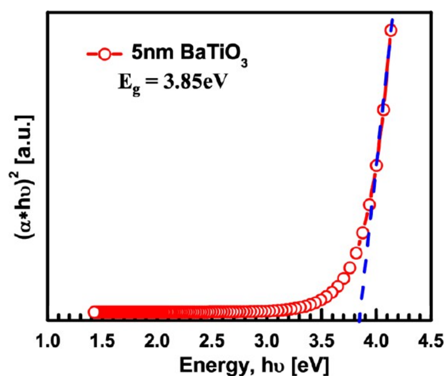

Figure 3. Absorption coefficient as a function of incident photon energy near the energy gap. The amorphous BTO band gap of 3.85 eV was determined from this plot.

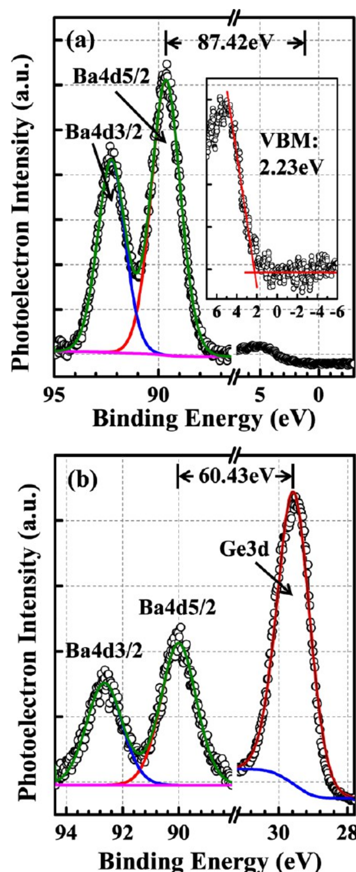

Figure 4. XPS spectra of (a) Ba $4d_{5/2}$ ($E^{Ba}_{Ba4d_{5/2}}$) core level, VBM (E^{Ba}_{VBM}) from 5 nm $BaTiO_3$ film, and (b) Ba $4d_{5/2}$ ($E^{Ba}_{Ba4d_{5/2}}$), Ge 3d (E^{Ge}_{Ge3d}) core levels from 1 nm $BaTiO_3$ film/(100)Ge interface, respectively.

RESULTS AND DISCUSSION

Material Characterization. Figure 1a−d shows the cross-sectional transmission electron microscopy (TEM) micrographs of the BTO/(110)Ge/(110)GaAs structure, showing the interface of Ge/(110)GaAs, the uniform thickness of BTO on Ge in a relative long range, the BTO/(110)Ge interface, and high-resolution TEM micrograph of the BTO/(110)Ge interface, respectively. These micrographs demonstrated the sharp interfaces between the GaAs and the Ge as well as the BTO and the Ge. Moreover, the TEM results demonstrated with a high degree of coherency of the pulse laser deposited ~5 nm thick amorphous BTO layer was grown on (110)Ge. One can also find from this Figure 1b that the interface of BTO/Ge is uniform, as needed to minimize the interface scattering of carrier transport from source to drain in a nanoscale transistor. Moreover, there is no unwanted low-κ interfacial layer[29] formed during the deposition of BTO on the (110)Ge layer and thus has a potential advantage of higher-κ BTO on (110)Ge to obtain better electrical transport characteristics, namely, equivalent oxide layer thickness, interface states, capacitance−voltage hysteresis, and frequency dispersion for low-power nanoscale transistor applications.

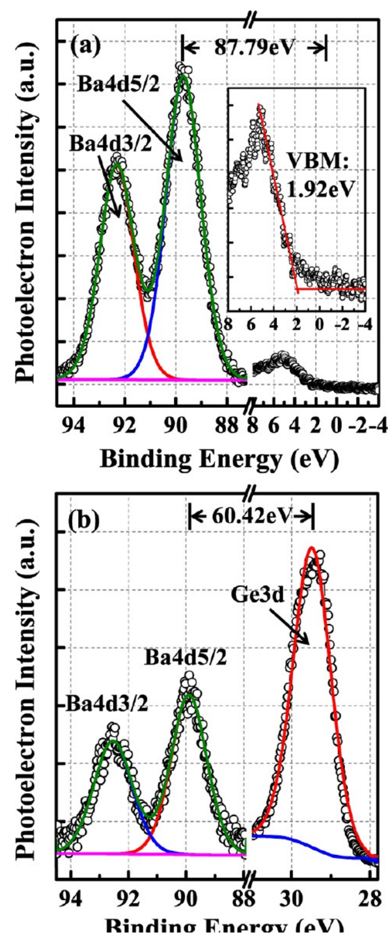

Figure 5. XPS spectra of (a) Ba $4d_{5/2}$ ($E^{Ba}_{Ba4d_{5/2}}$) core level, VBM (E^{Ba}_{VBM}) from 5 nm $BaTiO_3$ film, and (b) Ba $4d_{5/2}$ ($E^{Ba}_{Ba4d_{5/2}}$), Ge 3d (E^{Ge}_{Ge3d}) core levels from 1 nm $BaTiO_3$ film/(110)Ge interface, respectively.

Figure 2 shows high-resolution triple axis (004) symmetric X-ray rocking curves from the (002) Bragg line of 5 nmBTO/80 nm (110)Ge/(110)GaAs and 5 nmBTO/80 nm (111)Ge/(111)A GaAs structures. However, the X-ray rocking curve from (002) (not shown here) shows the appearance of strong Pendellösung oscillation fringes on both sides of BTO/Ge and GaAs peaks, which implies the presence of parallel and sharp heterointerfaces, similar to the perfectly lattice matched GaAs/Ge/GaAs heterostructure recently reported in ref 31. The interference fringes can only be observed in a structure that has almost perfectly parallel boundaries. The X-ray result also supports our cross-sectional TEM result of the amorphous nature of the BTO layer due to the absence of the BTO peak in the X-ray rocking curves.

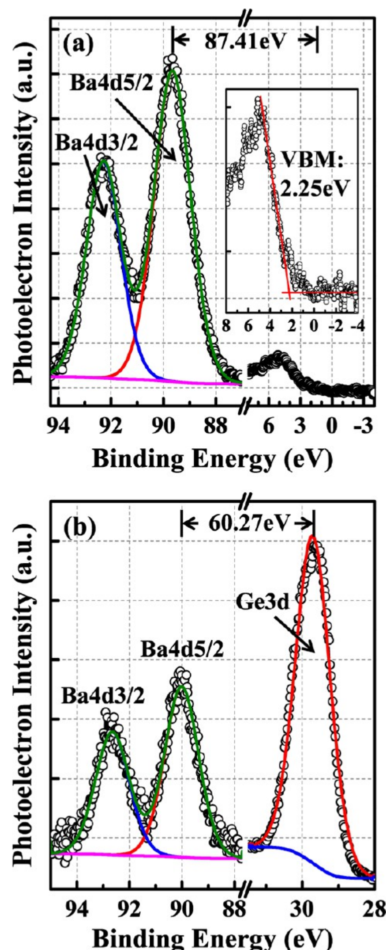

Figure 6. XPS spectra of (a) Ba $4d_{5/2}$ ($E^{Ba}_{Ba4d_{5/2}}$) core level, VBM (E^{Ba}_{VBM}) from 5 nm $BaTiO_3$ film, and (b) Ba $4d_{5/2}$ ($E^{Ba}_{Ba4d_{5/2}}$), Ge 3d (E^{Ge}_{Ge3d}) core levels from 1 nm $BaTiO_3$ film/(111)Ge interface, respectively.

The precise determination of the *band gap of amorphous thin* BTO is essential to determine the conduction band offset of BTO on crystallographically oriented Ge layers. The band gap of BTO was demonstrated in the literature from the bulk value of 3.4[32]−3.87 eV[33] of an ultrathin seven monolayer *c*-axis oriented tetragonal BTO layer. The absorption coefficient, α, is related to the band gap energy, E_g, as $(\alpha h\nu)^2 = A(h\nu - E_g)$, where A is a constant and the $h\nu$ is the incident photon energy. Figure 3 shows the $(\alpha h\nu)^2$ versus $h\nu$ graph of 5 nm BTO on (110)Ge, and by extrapolating the linear part of the data to the x axis of the graph, the band gap energy of 3.85 eV was determined, which is consistent with the reported result of an ultrathin BTO layer on a MgO substrate.[33] It is well-known that amorphous BTO is an insulating material with a resistivity of more than 10^{10} Ω·cm at room temperature and the mobility as low as 0.5 cm^2/V sec.[34,35] To determine the electrical band gap of BTO, the conductivity as a function of temperature is required. It has been reported that the temperature greater than 900 °C[34,35] is necessary for a meaningful electrical conductivity change that will enable the determination of the electrical band gap of single-crystal or polycrystalline BTO films. In the case of amorphous BTO, an even higher temperature is needed to change the electrical conductivity. However, in the Si CMOS process, and utilizing alternative channel materials such as Ge or compound semiconductors, the temperature needed for the determination of the electrical band gap of BTO is too high for the Ge/GaAs material system that can degrade the interface, interface intermixing, and material quality. Thus, the optical band gap of BTO is considered for the evaluation of the ΔE_C in this work.

Band Offset. The energy band alignment at the BTO/Ge heterointerface is of great importance, since the sufficient barriers for electron and hole are needed to suppress the tunneling leakage current in a nanoscale transistor using BTO as the gate dielectric. Also, the energy band alignment can provide a possibility for BTO to be used as a common gate dielectric for both Ge n- and p-channel nanoscale transistor applications. The valence band offset, ΔE_V, at the BTO on crystallographically oriented Ge layers was determined using the XPS system and angle integrated photoelectron energy distribution curves for the valence band maximum (VBM). Using these methods, Ge 3d and Ba $4d_{5/2}$ CL spectra were recorded, and the binding energy was corrected by adjusting the carbon (C) 1s core-level peak position to 285.0 eV for each sample surface. Figures 4−6 show XPS spectra of (a) Ba $4d_{5/2}$ ($E^{Ba}_{Ba4d_{5/2}}$) core level and VBM (E^{Ba}_{VBM}) from 5 nm thick BTO film on (100)Ge, (110)Ge, and (111)Ge and (b) Ge 3d core-level (E^{Ge}_{Ge3d}) and Ba $4d_{5/2}$ core-level ($E^{Ba}_{Ba4d_{5/2}}$) spectra from 1 nm BTO on (100)Ge, (110)Ge, and (111)Ge interfaces, respectively. The ΔE_V for a BTO on each Ge heterointerface was determined from the following equation[36] using CL spectra

$$\Delta E_v = (E^{Ge}_{Ge3d} - E^{Ge}_{VBM})^{Ge} - (E^{Ba}_{Ba4d_{5/2}} - E^{Ba}_{VBM})^{5nm\,BTO} - (E^{Ge}_{Ge3d} - E^{Ba}_{Ba4d_{5/2}})^{1nm\,BTO/Ge\,interface}$$

The band offset result would not change if we select Ba $4d_{3/2}$ as the CL binding energy peak since the separation of Ba $4d_{5/2}$ and Ba $4d_{3/2}$ peaks is fixed. Finally, the conduction band offset, ΔE_C, for BTO on each interface of Ge is determined from the following equation: $\Delta E_C = E_g^{BTO} - E_g^{Ge} - \Delta E_V$, where E_g^{BTO} and E_g^{Ge} are the band gaps of BTO and Ge, respectively.

The binding energy differences between the Ge 3d peak centroid and the VBM position of each crystallographically oriented Ge determined from the XPS measurements were $E^{Ge}_{Ge3d} - E^{Ge}_{VBM} = 29.45 \pm 0.05$ eV for (100)Ge, $E^{Ge}_{Ge3d} - E^{Ge}_{VBM} = 29.36 \pm 0.05$ eV for (110)Ge, and $E^{Ge}_{Ge3d} - E^{Ge}_{VBM} = 29.58 \pm 0.05$ eV for (111)Ge, respectively, reported earlier.[31] Similarly, the

Table 1. Core-Level to VBM Binding Energy Difference for $BaTiO_3$ and Epitaxial (100)Ge Grown on (100)/6° GaAs Substrate

material and interface	binding energy difference	measured band offsets of BTO/(100)Ge	
		ΔE_V (eV)	ΔE_C (eV)
Ge	$E^{Ge}_{Ge3d} - E^{Ge}_{VBM} = 29.45 \pm 0.005$ eV		
5 nm BTO	$E^{Ba}_{Ba4d_{5/2}} - E^{Ba}_{VBM} = 87.42 \pm 0.05$ eV		
1 nm BTO on Ge	$E^{Ba}_{Ba4d_{5/2}} - E^{Ge}_{Ge3d} = 60.43 \pm 0.05$ eV		
E_g of BTO	3.85 eV	2.46 ± 0.05	0.72 ± 0.05

Table 2. Core-Level to VBM Binding Energy Difference for $BaTiO_3$ and Epitaxial (110)Ge Grown on (110)GaAs Substrate

material and interface	binding energy difference	measured band offsets of BTO/(100)Ge	
		ΔE_V (eV)	ΔE_C (eV)
Ge	$E^{Ge}_{Ge3d} - E^{Ge}_{VBM}$ = 29.36 ± 0.05 eV		
5 nm BTO	$E^{Ba}_{Ba4d_{5/2}} - E^{Ba}_{VBM}$ = 87.79 ± 0.05 eV		
1 nm BTO on Ge	$E^{Ba}_{Ba4d_{5/2}} - E^{Ge}_{Ge3d}$ = 60.42 ± 0.05 eV		
E_g of BTO	3.85 eV	1.99 ± 0.05	1.19 ± 0.05

Table 3. Core-Level to VBM Binding Energy Difference for $BaTiO_3$ and Epitaxial (111)Ge Grown on (111)A GaAs Substrate

material and interface	binding energy difference	measured band offsets of BTO/(111)Ge	
		ΔE_V (eV)	ΔE_C (eV)
Ge	$E^{Ge}_{Ge3d} - E^{Ba}_{VBM}$ = 29.58 ± 0.05 eV		
5 nm BTO	$E^{Ba}_{Ba4d_{5/2}} - E^{Ba}_{VBM}$ = 87.41 ± 0.05 eV		
1 nm BTO on Ge	$E^{Ba}_{Ba4d_{5/2}} - E^{Ge}_{Ge3d}$ = 60.27 ± 0.05 eV		
E_g of BTO	3.85 eV	2.44 ± 0.05	0.74 ± 0.05

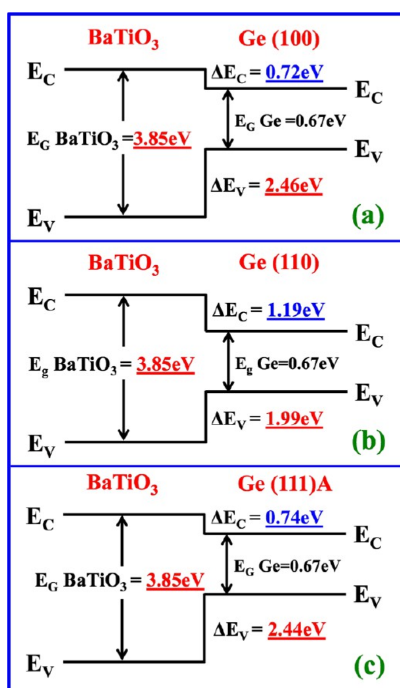

Figure 7. Energy band diagram of the $BaTiO_3$ on (a) (100)Ge, (b) (110)Ge, and (c) (111)Ge heterojunctions obtained from XPS measurements.

Table 4. Band Offset Values of $BaTiO_3$ on Crystallographically Oriented Epitaxial Ge Layers

	(100)	(110)	(111)
ΔE_V (eV)	2.46 ± 0.05	1.99 ± 0.05	2.44 ± 0.05
ΔE_C (eV)	0.72 ± 0.05	1.19 ± 0.05	0.74 ± 0.05
E_g of $BaTiO_3$ (eV)	3.85	3.85	3.85

energy differences between the Ba $4d_{5/2}$ centroid and the VBM for the 5 nm thick BTO film of each Ge layer are shown in Figures 4a, 5a, and 6a as well as tabulated in Tables 1−3.

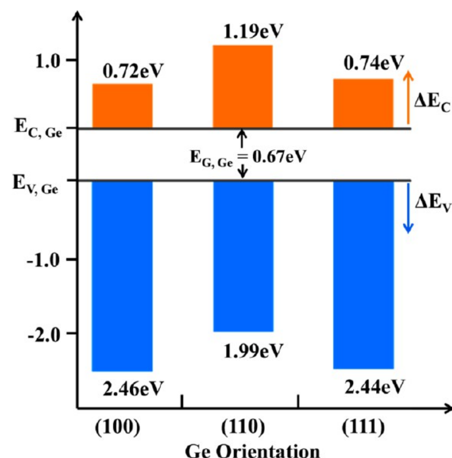

Figure 8. Histogram of band offset values of $BaTiO_3$ on crystallographically oriented (100)Ge, (110)Ge, and (111)Ge layers.

Furthermore, for the 1 nm BTO film on each Ge epilayer, the energy differences between the Ge 3d centroid and the Ba $4d_{5/2}$ CLs are also shown in Figures 4b, 5b, and 6b. Using these measured data and the equation above, the measured value of ΔE_V for BTO on (100)Ge, (110)Ge, and (111)Ge interfaces is 2.46 ± 0.05, 1.99 ± 0.05, and 2.44 ± 0.05 eV, respectively. The observed differences in the ΔE_V values for the BTO on crystallographically oriented Ge layers can be explained due to the difference in surface reconstruction of the Ge epilayers on GaAs substrates. As a result of the difference in surface reconstruction of Ge (i.e., (2×1), (2×2), (3×4), (1×1)),[36] the deposited band offset of BTO on crystallographically oriented epitaxial Ge would exhibit different values of band offsets. As the deposition temperature of BTO on Ge layers during the PLD process is lower than the crystallization temperature of BTO, the controlled incorporation of oxygen at the Ge interface during the deposition of BTO filled the dangling bonds of Ge. Oxygen can diffuse into Ge during the BTO growth process, but minimally due to the lower depostion temperature of 250 °C; however, there is no interfacial GeO_x layer formed between the BTO and the Ge layer, suggesting a robust heterointerface that prevents oxidation of the (110)Ge surface, similar to the case of HfO_2 on (110)Ge.[20,21] It has been reported that the band offset can also be dependent on the substrate orientation, surface reconstruction, deposition temperature, overlayer crystallinity, deposition rate, microscopic interface dipole, and interdiffusion or reactivity.[37] The calculated value of ΔE_C for BTO on (100)Ge, (110)Ge, and (111)Ge interface is 0.72 ± 0.05, 1.19 ± 0.05, and 0.74 ± 0.05 eV, respectively, using the measured 3.85 eV band gap of the BTO layer shown in Figure 3 and the well-known 0.67 eV band gap of Ge. Figure 7a−c shows the band alignment diagram of the BTO on (100)Ge, (110)Ge, and (111)Ge heterointerfaces, respectively, and the values are tabulated in Table 4. Figure 8

dx.doi.org/10.1021/am4036866 | ACS Appl. Mater. Interfaces 2013, 5, 11446−11452

shows the histogram of ΔE_V and ΔE_C distributions obtained from BTO on epitaxial (100)Ge, (110)Ge, and (111)Ge layers. One can find from this figure that the measured ΔE_V is above 1 eV, required for confining hole carriers inside the p-channel Ge to reduce the leakage current. It is also interesting to note that BTO can be used as a common gate dielectric for both p- and n-channel nanoscale transistors using Ge as a channel material operating at the gate voltage of 0.5 V.

CONCLUSIONS

In summary, a pulsed laser deposited perovskite $BaTiO_3$ layer on epitaxial crystallographically oriented Ge offers a new class of nanoscale transistors. Sharp interfaces between amorphous $BaTiO_3$ and the epitaxial Ge layer, without any interfacial layer as well as between the Ge and the GaAs substrate, are achieved. The band gap of 3.85 eV is measured in the amorphous $BaTiO_3$ layer. The valence band offset relation of $\Delta E_V(100) \geq \Delta E_V(111) > \Delta E_V(110)$ and the conduction band offset relation of $\Delta E_C(110) > \Delta E_C(111) \geq \Delta E_C(100)$ are demonstrated. The difference in band offsets on crystallographically oriented Ge is explained due to the difference in surface reconstruction of Ge on GaAs substrates. Higher than 1 eV of ΔE_V and ΔE_C on the (110)Ge layer as well as the ΔE_C band offsets higher than 0.5 eV on (100)Ge and (111)Ge will offer a common gate dielectric solution for the Ge-based p- and n-channel transistors at an operating voltage of 0.5 V. These band offset parameters for carrier confinement and the interface chemical properties of the $BaTiO_3$ on the crystallographically oriented nanostructured Ge system are necessary for designing Ge-based nanoscale transistors as well as perovskite/Ge-based multifunctional devices.

MATERIALS AND METHODS

Material Synthesis. The undoped epitaxial 80 nm thick Ge layers were grown using an in situ growth process on epi-ready polar (100)GaAs, nonpolar (110)GaAs, and polar (111)A GaAs substrates using separate solid source MBE growth chambers for Ge and III−V materials, connected via an ultra-high-vacuum transfer chamber. The growth temperature and growth rate of epitaxial Ge were 400 °C and 0.1 Å/s, respectively. The details of the growth procedure are reported elsewhere.[31,38] Epitaxial Ge layers were cleaned using $NH_4OH:H_2O_2:H_2O$ (2:1:1000 volume ratio) for 5 s prior loading to the PLD chamber for BTO deposition. The queue time was minimized between cleaning of the Ge layer and BTO deposition. The 1 and 5 nm BTO films were deposited by PLD using a KrF excimer laser (λ = 248 nm) on epitaxial (100)Ge, (110)Ge, and (111)Ge layers in two separate runs at a deposition rate of ~0.5 Å/s. The stoichiometric BTO target was synthesized by a conventional mixed-oxide processing route. The focused laser beam irradiates the rotating target at 89 rpm with a laser energy density of ~2.5 J/cm^2 at a repetition rate of 10 Hz. The deposition was made using a vacuum chamber with an oxygen pressure of 100 mTorr during the deposition of BTO films on epitaxial crystallographically oriented Ge layers. During the BTO growth, the substrate temperature of all Ge films was kept constant at 250 °C.

Materials Characterization. To determine the structural quality and the relaxation state of BTO on epitaxial Ge layers, high-resolution triple axis X-ray rocking curves were recorded. Cross-sectional high-resolution transmission electron microscopy (HR-TEM) was used to characterize the interface between the BTO and the Ge epilayer. HR-TEM imaging was performed using an FEI Titan 80-300 transmission electron microscope. For this purpose, the electron transparent foils of thin film cross sections of $BaTiO_3$/Ge/(110)GaAs were prepared by a standard polishing technique, i.e., mechanical grinding, dimpling, and Ar^+-ion beam-milling. The band gap of the BTO layer on Ge was determined from optical dispersion collected using variable-angle spectroscopic ellipsometry. The band alignment of BTO on each Ge layer was investigated using a PHI Quantera SXM XPS system with a monochromated Al Kα (energy of 1486.7 eV) X-ray source. The Ge 3d and Ba $4d_{5/2}$ core-level (CL) binding energy spectra as well as Ge and Ba valence band binding energy spectra were collected with a pass energy of 26 eV and an exit angle of 45°. The binding energy was corrected by adjusting the carbon (C) 1s CL peak position to 285.0 eV for each sample surface. Curve fitting was performed by the CasaXPS 2.3.14 using a Lorentzian convolution with a Shirley-type background. The CL energy position was defined to be the center of the peak width at the half of the peak height. The VBM values were determined by linear extrapolation of the leading edge to the base line of the valence band spectra recorded for the 5 nm BTO and each Ge layer to the base lines. The VBM value is sensitive to the choice of points on the leading edge used to obtain the regression line. The uncertainties of ΔE_V and ΔE_C values were found to be in the range of 0.05−0.1 eV in the present work by the regression analysis of selected data over the linear region.

AUTHOR INFORMATION

Corresponding Author

*E-mail: mantu.hudait@vt.edu. Tel: (540) 231-6663. Fax: (540) 231-3362.

Notes

The authors declare no competing financial interest.

ACKNOWLEDGMENTS

This work is supported in part by National Science Foundation under grant number ECCS-1348653 and Intel Corporation. The authors (S.P., D.M., and R.V.) acknowledge the financial support from the Office of Basic Energy Science, Department of Energy, through grant no. DE-FG02-06ER46290.

REFERENCES

(1) Jia, C.; Chen, Y.; Guo, Y.; Liu, X.; Yang, S.; Zhang, W.; Wang, Z. *Nanoscale Res. Lett.* **2011**, *6*, 316−320.
(2) Liang, Y.; Curless, J.; McCready, D. *Appl. Phys. Lett.* **2005**, *86*, 082905−082907.
(3) Voora, V. M.; Hofmann, T.; Schubert, M.; Brandt, M.; Lorenz, M.; Grundmann, M.; Ashkenov, N.; Schubert, M. *Appl. Phys. Lett.* **2009**, *94*, 142904.
(4) Voora, V. M.; Hofmann, T.; Brandt, M.; Lorenz, M.; Grundmann, M.; Ashkenov, N.; Schmidt, H.; Ianno, N.; Schbert, M. *Phys. Rev B* **2010**, *81*, 195307−195318.
(5) Losego, M. D.; Kourkoutis, L. F.; Mita, S.; Craft, H. S.; Muller, D. A.; Collazo, R.; Sitar, Z.; Maria, J. P. *J. Cryst. Growth* **2009**, *311*, 1106−1109.
(6) Brandt, M.; Frenzel, H.; Hochmuth, H.; Lorentz, M.; Grundmann, M.; Schubert, J. *J. Vac. Sci. Technol., B* **2009**, *27*, 1789−1793.
(7) Jia, C. H.; Chen, Y. H.; Zhou, X. L.; Liu, G. H.; Guo, Y.; Liu, X. L.; Yang, S. Y.; Wang, Z. G. *J. Cryst. Growth* **2010**, *312*, 373−377.
(8) Chambers, S. A.; Droubay, T.; Kaspar, T. C.; Gutowski, M. *J. Vac. Sci. Technol., B* **2004**, *22*, 2205−2215.
(9) Contreras-Guerrero, R.; Veazey, J. P.; Levy, J.; Droopad, R. *Appl. Phys. Lett.* **2013**, *102*, 012907.
(10) McKee, R. A.; Walker, F. J.; Chisholm, M. F. *Science* **2001**, *293*, 468−471.
(11) Merckling, C.; Saint-Girons, G.; Botella, C.; Hollinger, G.; Heyns, M.; Dekoster, J.; Caymax, M. *Appl. Phys. Lett.* **2011**, *98*, 092901.
(12) Salahuddin, S.; Datta, S. *Nano Lett.* **2008**, *8*, 405−410.
(13) Krowne, C. M.; Kirchoefer, S. W.; Chang, W.; Pond, J. M.; Alldredge, L. M. B. *Nano Lett.* **2011**, *11*, 988−992.
(14) *International Technology Roadmap for Semiconductors (ITRS)*, 2011 ed.; 2011; Process Integration, Devices, and Structures (PIDS) Chapter.
(15) Hsieh, B.-F.; Chang, S.-T. *Solid-State Electron.* **2011**, *60*, 37−41.

(16) Lee, C. H.; Nishimura, T.; Saido, N.; Nagashio, K.; Kita, K.; Toriumi, A. *IEEE Conference Proceedings of the International Electron Devices Meeting (IEDM)*; IEEE: New York, 2009; pp 457−460.
(17) Dissanayake, S.; Zhao, Y.; Sugahara, S.; Takenaka, M.; Takaghi, S. *J. Appl. Phys.* **2011**, *109*, 033709.
(18) Yang, Y. J.; Ho, W. S.; Haung, C. F.; Chang, S. T.; Liu, C. W. *Appl. Phys. Lett.* **2007**, *91*, 102103.
(19) Krishnamohan, T.; Kim, D.; Dinh, T. V.; Pham, A.; Meinerzhagen, B.; Jungemann, C.; Saraswat, K. *IEEE Conference Proceedings of the International Electron Devices Meeting (IEDM)*; IEEE: New York, 2008; pp 899−892.
(20) Hudait, M. K.; Zhu, Y.; Maurya, D.; Priya, S. *Appl. Phys. Lett.* **2013**, *102*, 093109.
(21) Hudait, M. K.; Zhu, Y. *J. Appl. Phys.* **2013**, *113*, 114303.
(22) Perego, M.; Seguini, G.; Fanciulli, M. *J. Appl. Phys.* **2006**, *100*, 093718.
(23) Choi, J. H.; Mao, Y.; Chang, J. P. *Mater. Sci. Eng. Rep.* **2011**, *R72*, 97−136.
(24) Swaminathan, S.; Sun, Y.; Pianetta, P.; McIntyre, P. C. *J. Appl. Phys.* **2011**, *110*, 094105.
(25) Robertson, J. *Eur. Phys. J.: Appl. Phys.* **2004**, *28*, 265−291.
(26) Ponath, P.; Posadas, A.; Fredrickson, K.; Kvit, A.; Demkov, A. Epitaxial Growth of $BaTiO_3$ on Ge. In *Bulletin of the American Physical Society: APS March Meeting*, March 18−22, 2013, Baltimore, MD; 2013.
(27) Hudait, M. K.; Zhu, Y.; Maurya, D.; Priya, S.; Patra, P. K.; Ma, A. W. K.; Aphale, A.; Macwan, I. *J. Appl. Phys.* **2013**, *113*, 134311.
(28) Hudait, M. K.; Zhu, Y.; Jain, N.; Maurya, D.; Zhou, Y.; Priya, S. *J. Appl. Phys.* **2013**, *114*, 024303.
(29) McKee, R. A.; Walker, F. J.; Chisholm, M. F. *Phys. Rev. Lett.* **1998**, *81*, 3014−3017.
(30) Elshocht, S. V.; Brijs, B.; Caymax, M.; Conard, T.; Chiarella, T.; Gendt, S. D.; Jaeger, B. D.; Kubicek, S.; Meuris, M.; Onsia, B.; Richard, O.; Teerlinck, I.; Steenbergen, J. V.; Zhao, C.; Heyns, M. *Appl. Phys. Lett.* **2004**, *85*, 3824.
(31) Hudait, M. K.; Zhu, Y.; Jain, N.; Hunter, J. L., Jr. *J. Vac. Sci. Technol.* **2013**, *B31*, 11206−11219.
(32) Jellison, G. E., Jr.; Boatner, L. A.; Lowndes, D. H.; McKee, R. A.; Godbole, M. *Appl. Opt.* **1994**, *33*, 6053−6058.
(33) Guo, H.; Liu, L.; Chen, Z.; Ding, S.; Lu, H.; Jin, K.-J.; Zhou, Y.; Cheng, B. *Europhys. Lett.* **2006**, *73*, 110−115.
(34) Heywang, W. *J. Mater. Sci.* **1971**, *6*, 1214−1226.
(35) Long, S. A.; Blumenthal, R. N. *J. Am. Ceram. Soc.* **1971**, *54*, 515−519.
(36) Kraut, E. A.; Grant, R. W.; Waldrop, J. R.; Kowalczyk, S. P. *Phys. Rev. Lett.* **1980**, *44*, 1620−1623.
(37) Brillson, L. J. *Surfaces and Interfaces of Electronic Materials*; Wiley-VCH: Weinheim, Germany, 2010.
(38) Hudait, M. K.; Zhu, Y.; Jain, N.; Vijayaraghavan, S.; Saha, A.; Merritt, T.; Khodaparast, G. A. *J. Vac. Sci. Technol.* **2012**, *B30*, 51205−51215.